

Long-Range Optical Wireless Information and Power Transfer

Yunfeng Bai, Qingwen Liu, *Senior Member, IEEE*, Riqing Chen, *Member, IEEE*, Qingqing Zhang, and Wei Wang

Abstract—Simultaneous wireless information and power transfer (SWIPT) is a remarkable technology to support both the data and the energy transfer in the era of Internet of Things (IoT). In this paper, we propose a beam-compression resonant beam (BCRB) system for long-range optical wireless information and power transfer based on the telescope internal modulator (TIM). Utilizing the TIM, the resonant beam is compressed, making the beam be further concentrated. Thus, the transmission loss produced by the beam diverged will decrease, which enables the long-range SWIPT capability. We establish the analytical model of the BCRB system including end-to-end beam transmission, beam spot radius, the energy output power, and the spectral efficiency. Based on it, the performance on the beam-compression, energy delivery, and data transfer have been evaluated, and the influence of structure parameters on it has been analyzed. Numerical results illustrate that the exemplary BCRB system can deliver 6 W power and have 18 bit/s/Hz spectral efficiency over 200 m distance.

Index Terms—Simultaneous wireless information and power transfer, Resonant beam, Long-range, Internet of Things

I. INTRODUCTION

In the era of Internet of Things (IoT), countless network devices are interconnected in various scenarios for making our life smart and convenient. However, with expansion of applications of IoT, their demands for communication and power increase dramatically [1]–[5]. Facing this bottleneck, simultaneous wireless information and power transfer (SWIPT) technology has recently attracted wide attention to providing both information and energy at the same time [6]. SWIPT technologies can be classified into two types: wide-area omnidirectional and narrow-beam orientation. Wide-area omnidirectional technology such as broadcasting radio-wave can support long-distance and omnidirectional SWIPT [7]. But, the broadcasting energy emission results in energy dissipation, which makes it difficult to achieve high-power transmission. Narrow-beam orientation technology such as beamforming light-emitting diode/laser diode can support high energy density transmission [8]. But using the narrow electromagnetic beam always accompanies the challenges of alignment and human safety.

Y. Bai, and Q. Liu, are with the College of Electronic and Information Engineering, Tongji University, Shanghai, 201804, China, (email: baiyf@tongji.edu.cn, qliu@tongji.edu.cn).

Riqing Chen is with the Digital Fujian Institute of Big Data for Agriculture and Forestry, Fujian Agriculture and Forestry University, Fuzhou, P.R. China. (e-mail: riqing.chen@fafu.edu.cn).

W. Wang is with the Shanghai Institute of Optics and Fine Mechanics, Chinese Academy of Sciences, Shanghai, China. (email: wangwei2016@siom.ac.cn).

Qingqing Zhang is with the School of Electronic Information and Communications, Huazhong University of Science and Technology, Wuhan 430074, China (e-mail: q_zhang@hust.edu.cn).

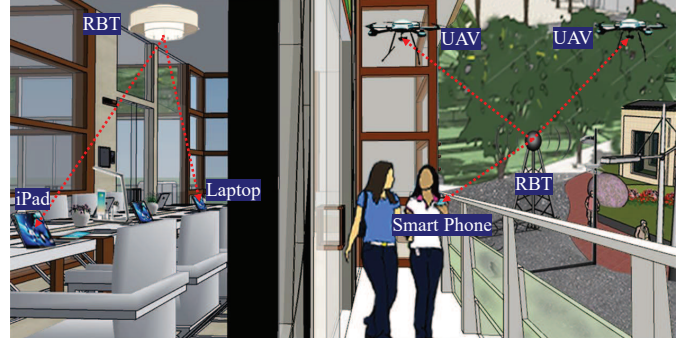


Fig. 1. Resonant beam systems application scenarios (RBT: resonant beam transmitter; UAV: unmanned aerial vehicle)

To meet the requirements of high power, safety, and mobility, a resonant beam (RB) SWIPT scheme has been proposed [9].

The scheme utilizes the optical beam as the energy and data carrier, which belongs to the narrow-beam type for high power transmission. Moreover, due to the end-to-end line of sight (LoS) characteristic, the beam transmission will cease immediately when objects intrusion, which ensures safety. Besides, due to the separation cavity structure and retro-reflectors, the system can realize self-alignment for mobility [10]. Furthermore, the optical carrier of resonant beam enables the ability of high-rate data transfer due to huge available bandwidth and high signal-to-noise ratio [11]. Fig. 1 depicts the application scenarios of the RB system. Devices such as the unmanned aerial vehicle (UAV), smartphones, laptops, etc., can be supported by it [12].

The idea of the RB system was firstly proposed in [9] and analyzed in [13]. Since then, related reports about the RB have been put forward one after another. An adaptive RBC (ARBC) system for battery charging optimization was proposed in [14]. A system has been demonstrated to achieve 2 W power transfer over 2.6 m distance in lab test [15]. An analytical model to depict information transfer in the RB system has been established in [16]. A time-division multiple access (TDMA) method was put forward to support multi-user scenarios [17]. A first-access-first-charge (FAFC) scheduling algorithm was proposed to keep all devices working as long as possible for fairness [18]. A design was presented in [10] to demonstrate the mobility of the RB system based on retro-reflectors. An analytical model based on the electromagnetic field was established for assessing the safety of the RB system [19]. The above research has explored the system structures and theoretical principles of RB, which reveals its application prospect. However, the transmission distance of the original RB scheme in literature can only achieve a few

meters, which make it face the challenge of being adopted in scenarios such as large warehouses and outdoor spaces. In this paper, to enhance the transmission distance, we propose a beam-compression RB scheme based on the telescope internal modulator (TIM). Through the beam compressed by the TIM, the incident beam on the gain can effectively enter without beam loss, which greatly reduces the overall transmission loss, making the long-range SWIPT possible.

The contributions of this paper are as follows:

- A beam-compression resonant beam (BCRB) system scheme based on the telescope internal modulator (TIM) is proposed, which can achieve long-range optical wireless information and power transfer.
- An analytical model of the BCRB system is established, which can depict the end-to-end beam transmission, beam spot radius, energy output, and data receiving ability. It is supplied a practical approach for evaluating system performance as well as guidelines for parameter optimization.

The presentation of the system fundamental concept will be illustrated in Section II of the rest of this paper. The BCRB system's analytical model will be developed in Section III. The performance of the BCRB system will be evaluated in Section IV. Finally, in Section V, conclusions will be drawn.

II. SYSTEM FUNDAMENTAL PRINCIPLE

Fig. 2 depicts a schematic representation of the BCRB system. The system is made up of two parts: the transmitter and the receiver, which are separated by space. A reflector M1, a power source, a gain medium, and a TIM are all part of the transmitter. A reflector M2, a beam splitter, a photovoltaic (PV) cell, and an avalanche photodiode are all part of the receiver (APD). The spatially separated laser resonator (SSLR) cavity is formed by the reflectors M1, M2, and the gain medium, and it is utilized to create and transmit the resonant beam. In the following subsections, we will briefly outline the fundamental principles of system energy transfer and communication, as well as assess the factors that influence system transmission distance.

A. Beam Output

The system's energy conversion process is separated into three phases: energy absorption, stimulated emission, and beam output. 1) *Energy absorption*: The input electrical power is converted to pump beam power in the power source. Then, with the pump beam radiating to the gain medium, the particles in the gain medium will be activated, which leads the particles being transited from low energy level to high energy level. Finally, population inversion occurs and energy is stored in the gain medium. 2) *Stimulated radiation*: Particles are continually transited to the high energy level with the pump power input. Because high-energy particles are in the unstable state, they will fall back to a lower energy level with spontaneous and stimulated radiation and produce photons. 3) *Beam output*: These released photons will travel between the reflectors M1 and M2, accompanied by energy gain and loss. Finally, beam output from M2.

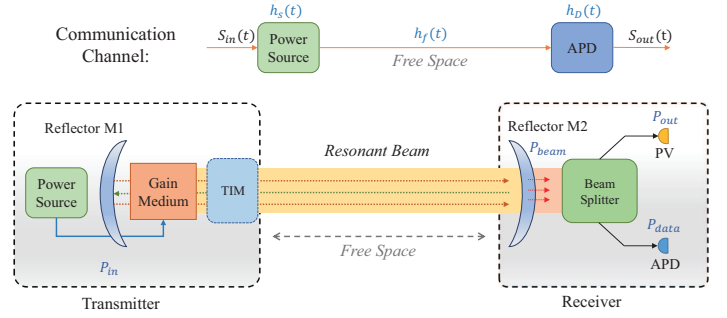


Fig. 2. System diagram (TIM: telescope internal modulator; PV: photovoltaic; APD: avalanche photodiode)

B. Signal Delivering

The data signal is loaded on the pump beam by modulating the power source, as shown in Fig. 2. The gain medium receives the pump beam and generates the excitation beam. Due to the mapping relationship between the pump beam and the excitation beam, the signal can be delivered into the resonant cavity. Finally, with the beam transmitting through the free space from transmitter to receiver, the signal will be received by the APD detector. Overall, the communication process of the proposed system is similar to traditional space optical communication, which can be modeled as a linear time-invariant system [20]:

$$s_{out}(t) = h_s(t) * h_f(t) * h_D(t) * P_{data} s_{in}(t) + n_t(t), \quad (1)$$

where $n(t)$ is the additive white Gaussian noise (AWGN), and $h_s(t)$, $h_f(t)$, and $h_D(t)$ are the impulse response functions of the adjustable power source, the free space and the APD detector, respectively.

C. Transmission Loss

Energy loss affects the output performance of the system, such as heat loss, air absorption loss, optical reflection loss, and beam diffraction loss. Among them, beam diffraction loss belong to transmission loss which will gain as the distance increase, impacting the beam transfer range. According to [21], the beam diffraction loss comes from the beam diffraction and overflow on the finite aperture. As can be seen in Fig. 3, the beam spreads in open space, with a divergence angle θ and beam spot (beam cross-section) radius ω . Due to θ , the beam will inevitably diffusion during transmission, which makes the spot radius enlarge from ω to ω' . When there is an aperture with radius a ($a < \omega'$) in the transmission route, a portion of the beam will overflow or become obstructed, resulting in beam loss. Furthermore, because the beam divergence increases with distance, the loss will increase, continuously. The beam transmission will be cut off when the energy loss is big enough over a given distance. Generally, if the beam spot is substantially bigger than the aperture, significant energy loss will present. In contrast, energy loss will be minimal if the beam spot is manageable and the majority of the beam may travel through the aperture instead of being obstructed or overflowing [22], [23].

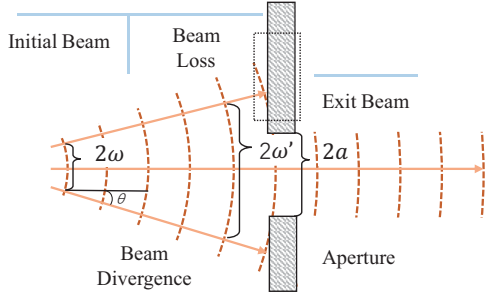


Fig. 3. Beam loss on aperture (ω : initial beam radius; ω' : divergent beam radius; a : aperture radius; θ : divergence angle)

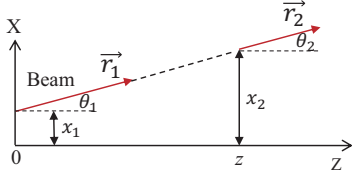


Fig. 4. Beam propagating in the free space (\vec{r}_1 :beam with location x_1 and θ_1 angle; \vec{r}_2 :beam with location x_2 and θ_2 angle; z : \vec{r}_2 location on the Z axis)

In the RB system, several elements such as gain medium and reflectors with geometric boundary exist in the transmission route. Among them, gain medium for beam generation has the minimum size, which is the major influence factor for the transmission distance. On this premise, TIM was proposed and introduced into the proposed scheme. Detailed analysis models will be described in the next chapter.

III. ANALYTICAL MODEL

In this section, will develop the end-to-end beam transmission model at first, including the transmission matrix for beam propagation describing and stable transmission condition for cavity evaluating. Then, we will establish the beam radius model for evaluating the compression performance of the TIM. In the rest, the energy harvesting and data receiving models will be presented. These models lay an analytical foundation for the performance evaluation of the BCRB system in Section IV.

A. End-to-end Beam Transmission

1) *Transmission matrix*: To establish the analytical model of the beam transmission, the propagation of the beam between the transmitter and the receiver should be depicted in mathematical. Based on [23], we introduce the beam vector

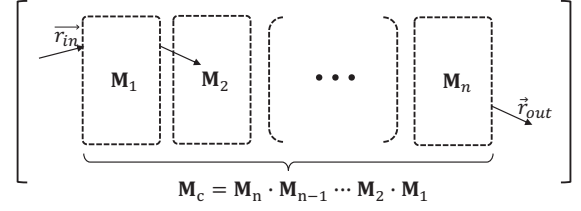


Fig. 5. Beam propagation in concatenate elements (\vec{r}_{in} : Initial beam vector; \vec{r}_{out} : Exit beam vector; \mathbf{M}_1 - \mathbf{M}_n : transmission matrices)

and transmission matrix to accurately and strictly analyze the beam transfer. Fig. 4 shows the process of beam propagating straightly in the air. The incident beam is denoted by $\vec{r}_1 = (x_1, \theta_1)$, where x_1 is the start point location and θ_1 is the inclination angle. The beam travels along the dotted line and comes to position z . Taking the \vec{r}_2 representing the beam at z , its beam parameters are set as (x_2, θ_2) . After the beam propagating, the vector \vec{r}_1 converts to $\vec{r}_2 = (x_2, \theta_2)$. Considering the beam travels in a straight line, parameters' relationship between the \vec{r}_1 and \vec{r}_2 can be described as:

$$\begin{cases} \theta_2 = \theta_1 \\ x_2 = x_1 + z \tan \theta_1 \end{cases} \quad (2)$$

Normally, the beam transmits off the light axis (Z) in the system. Thus, the inclination angle can be small, which satisfies $\tan \theta_1 \approx \theta_1$. At the moment, the vectors could be represented as:

$$\vec{r}_2 = \begin{bmatrix} 1 & z \\ 0 & 1 \end{bmatrix} \vec{r}_1 = \mathbf{M}_z \vec{r}_1, \quad (3)$$

where the \mathbf{M}_z is denoted as the transmission matrix. Generally, the transmission matrix can be expressed as:

$$\mathbf{M} = \begin{bmatrix} A & B \\ C & D \end{bmatrix}, \quad (4)$$

where A, B, C, D are matrix elements determined by the medium structure.

Usually, different optical mediums will exist in the cavity with different transmission matrices, such as lenses, reflectors. The situation that the beam passed multi-mediums is depicted in Fig. 5. The beam vector \vec{r}_{in} starts on the left. After passing the first medium, \vec{r}_{in} is converted to \vec{r}_{out} and so next. If the space has n mediums with matrices $\mathbf{M}_1 \sim \mathbf{M}_n$, \vec{r}_{in} is finally converted to \vec{r}_{out} as:

$$\vec{r}_{out} = \mathbf{M}_n \cdots \mathbf{M}_2 \mathbf{M}_1 \vec{r}_{in} = \mathbf{M}_c \vec{r}_{in}, \quad (5)$$

where \mathbf{M}_c is concatenated by $\mathbf{M}_1 \sim \mathbf{M}_n$.

TABLE I
MATRIX EXPRESSION

\mathbf{M}_{M1}	\mathbf{M}_{M2}	\mathbf{M}_{D1}	\mathbf{M}_{D2}	\mathbf{M}_{L1}	\mathbf{M}_{L2}	\mathbf{M}_{L3}	\mathbf{M}_l
$\begin{bmatrix} 1 & 0 \\ -\frac{1}{\rho_1} & 1 \end{bmatrix}$	$\begin{bmatrix} 1 & 0 \\ -\frac{1}{\rho_2} & 1 \end{bmatrix}$	$\begin{bmatrix} 1 & 0 \\ -\frac{1}{f_1} & 1 \end{bmatrix}$	$\begin{bmatrix} 1 & 0 \\ -\frac{1}{f_2} & 1 \end{bmatrix}$	$\begin{bmatrix} 1 & L_1 \\ 0 & 1 \end{bmatrix}$	$\begin{bmatrix} 1 & L_2 \\ 0 & 1 \end{bmatrix}$	$\begin{bmatrix} 1 & L_3 \\ 0 & 1 \end{bmatrix}$	$\begin{bmatrix} M & 0 \\ 0 & \frac{1}{M} \end{bmatrix}$

2) *Stable transmission condition*: The stable transmission condition must be satisfied when designs the system, as it determines whether the beam will overflow when propagating between the transmitter and the receiver [23].

Since the transmission matrix has been developed, we can use it to describe the beam propagation in one round-trip (end-to-end). In the BCRB system, taking the position of the beam at M1 as the starting point, the beam will pass through M1, the gain medium, the convex lens and concave lens to M2 in succession. Based on [Section I.A.1)], the beam propagation can be depicted by transmission matrix as:

$$\begin{aligned} \mathbf{M}_{\text{RT}} &= \mathbf{M}_{\text{M1}} \mathbf{M}_{L_1} \mathbf{M}_{L_2} \mathbf{M}_{D_1} \mathbf{M}_l \mathbf{M}_{D_2} \mathbf{M}_{L_3} \mathbf{M}_{\text{M2}} \\ &\quad \cdot \mathbf{M}_{L_3} \mathbf{M}_{D_2} \mathbf{M}_l \mathbf{M}_{D_1} \mathbf{M}_{L_2} \mathbf{M}_{L_1} \\ &= \begin{bmatrix} A_{\text{RT}} & B_{\text{RT}} \\ C_{\text{RT}} & D_{\text{RT}} \end{bmatrix}, \end{aligned} \quad (6)$$

where \mathbf{M}_{M1} , \mathbf{M}_{M2} , \mathbf{M}_{D_1} , \mathbf{M}_{D_2} and \mathbf{M}_l represent the transmission sub-matrix of beam propagating through the reflector M1, M2, and the TIM (D_1 and D_2 : lenses; l : lenses' distance); \mathbf{M}_{L_1} , \mathbf{M}_{L_2} , and \mathbf{M}_{L_3} are introduced to depict the process of the beam passing the air with different space distance L_1 , L_2 and L_3 . The matrix expressions of $\mathbf{M}_{\text{M1}} \sim \mathbf{M}_{L_3}$ have been presented in TABLE I [22]–[24]. Note that the gain medium normally makes by high transmittance material. Thus, we can amuse that it follows the same transmission law like the air medium.

Furthermore, to get the stable condition, we consider the situation that the beam has transmitted n times in the cavity, which is:

$$\vec{r}_n = \mathbf{M}_{\text{RT}} \cdots \mathbf{M}_{\text{RT}} \mathbf{M}_{\text{RT}} \vec{r}_0 = \mathbf{M}_{\text{RT}}^n \vec{r}_0, \quad (7)$$

where $\vec{r}_0 = (x_0, \theta_0)$ is the initial beam vector, $\vec{r}_n = (x_n, \theta_n)$ is the end beam vector. According to Sylvester's theorem, \mathbf{M}_{RT}^n satisfies the following formula:

$$\begin{aligned} \mathbf{M}_{\text{RT}}^n &= \begin{bmatrix} A_{\text{RT}} & B_{\text{RT}} \\ C_{\text{RT}} & D_{\text{RT}} \end{bmatrix}^n = \begin{bmatrix} A_{\text{RT},n} & B_{\text{RT},n} \\ C_{\text{RT},n} & D_{\text{RT},n} \end{bmatrix} \\ &= \frac{1}{\sin \Theta} \cdot \\ &\quad \begin{bmatrix} A_{\text{RT}} \sin n\Theta - \sin(n-1)\Theta & B_{\text{RT}} \sin n\Theta \\ C_{\text{RT}} \sin n\Theta & D_{\text{RT}} \sin n\Theta - \sin(n-1)\Theta \end{bmatrix}, \end{aligned} \quad (8)$$

where

$$\Theta = \arccos \frac{1}{2}(A_{\text{RT}} + D_{\text{RT}}). \quad (9)$$

At this moment, \vec{r}_n can be depicted as:

$$\begin{cases} x_n = A_{\text{RT},n} x_0 + B_{\text{RT},n} \theta_0 \\ \theta_n = C_{\text{RT},n} x_0 + D_{\text{RT},n} \theta_0 \end{cases}. \quad (10)$$

When the system is stable, the beam will not overflow after n times of cyclicly transmission, which means the value of $|\vec{r}_n|$ should be limited ($|\cdot|$ =vector modulus). Thus, the value of $A_{\text{RT},n}$, $B_{\text{RT},n}$, $C_{\text{RT},n}$, and $D_{\text{RT},n}$ must be controlled at any n . Therefore, the value of Θ should be a real number, where A_{RT} and D_{RT} satisfy the inequality as:

$$-1 < \frac{1}{2}(A_{\text{RT}} + D_{\text{RT}}) < 1. \quad (11)$$

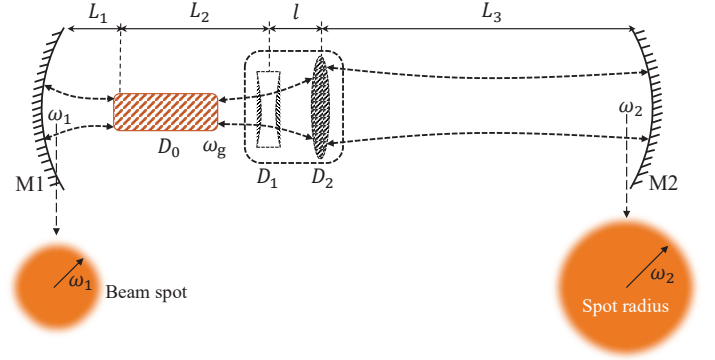


Fig. 6. Parameters Diagram of BCRB System ($\omega_1 \sim \omega_3$: beam spot radius; $L_1 \sim L_3$: elements' distance; D_0 : gain medium; D_1 , D_2 : lens; M1, M2: reflector)

Doing the matrix calculation for (6) and taking the matrix elements from \mathbf{M}_{RT} into (11), the following inequality can be obtained as:

$$\begin{aligned} 0 &< \left(\frac{f_2}{f_1} + \frac{l - (L_1 + L_2) \frac{f_2}{f_1} - \frac{L_3 f_1}{f_2}}{\rho_1} \right) \\ &\quad \cdot \left(\frac{f_1}{f_2} + \frac{l - (L_1 + L_2) \frac{f_2}{f_1} - \frac{L_3 f_1}{f_2}}{\rho_2} \right) < 1 \end{aligned} \quad (12)$$

From (12), comparing with the original system, three additional parameters l , f_1 and f_2 brought from TIM will impact the end-to-end transmission matrix of BCRB system. Through changing these parameters, the transmission matrix is adjusted, and the beam propagation can be changed for different demand, correspondingly. Based on it, substituting fixed boundary parameters and combining control variate, the restriction condition of the characteristic parameter such as the theoretical maximum distance can be determined.

B. Beam Spot Radius

From section II.C, we know that the beam loss will occur on the gain medium because of the beam divergence. A TIM is introduced in the transmission path for compressing the incident beam and inhibit the beam loss. The beam change should be analyzed.

The beam spot is the intensity distribution of the beam's cross-section, we can use its radius to judge the beam's change. In section III.A, we have developed the beam transmission matrix \mathbf{M}_{RT} which can depict the beam propagation in BCRB system. Based on it and [25], the beam spot radius on the gain can be given by:

$$\omega_g \approx \omega_{\text{M1}} = \sqrt{\frac{\lambda}{\pi}} \sqrt{\frac{\xi^2 \zeta_2}{\zeta_1 (1 - \zeta_1 \zeta_2)}}, \quad (13)$$

where ω_{M1} represent the beam mode radius on the M1; λ is the wavelength of the resonant beam; ζ_1 , ζ_2 , and ξ are

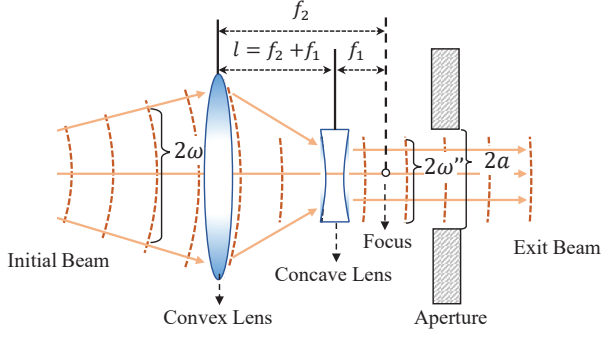


Fig. 7. Beam compressed by TIM (ω : initial beam radius; ω' : compressed beam radius; a : aperture radius; f_2 : focal length of convex lens ($f_2 > 0$); f_1 : focal length of concave lens ($f_1 < 0$); l distance of two lenses)

intermediate variables, which are defined as:

$$\begin{cases} \zeta_1 = \frac{f_2}{f_1} + \frac{l - (L_1 + L_2)\frac{f_2}{f_1} - \frac{L_3 f_1}{f_2}}{\rho_1} \\ \zeta_1 = \frac{f_1}{f_2} + \frac{l - (L_1 + L_2)\frac{f_2}{f_1} - \frac{L_3 f_1}{f_2}}{\rho_2} \\ \xi = l - (L_1 + L_2)\frac{f_2}{f_1} - \frac{L_3 f_1}{f_2} \end{cases} \quad (14)$$

Since L_1 and the length of the gain medium are short and far less than the transmission distance L_3 , the beam divergence over this short distance can be negligible. Therefore, the beam spot on the gain medium ω_g can be approximately equal to ω_{M1} , which simplifies the calculation process.

From the analysis above, we know the fact that beam divergence will cause transmission loss. Thus, if the beam can be compressed before it enters the aperture, transmission loss can be restrained. Fig. 7 shows the schematic of the TIM and the process of the beam compression. The TIM is composed by a concave lens and a convex lens, and their focal length is $-f_1$ and f_2 . Two lenses are placed in parallel, and their focuses are overlap ($l = f_1 + f_2$) [26]. When the resonant beam enters the TIM, it will first pass the convex lens. Under the function of the lens, the phase of the beam is changed, which makes the beam transmit toward the lens's focal point. Then, the beam passes the concave lens, and a second phase change is undergone, which leads the beam parallelly emitting from the concave lens. Through the transmission matrix, these process can be expressed as:

$$\begin{aligned} \mathbf{M}_{D_2} \mathbf{M}_l \mathbf{M}_{D_1} &= \begin{bmatrix} 1 & 0 \\ -\frac{1}{f_2} & 1 \end{bmatrix} \begin{bmatrix} 1 & l \\ 0 & 1 \end{bmatrix} \begin{bmatrix} 1 & 0 \\ -\frac{1}{f_1} & 1 \end{bmatrix} \\ &= \begin{bmatrix} \frac{1}{M} & l \\ 0 & M \end{bmatrix}, \end{aligned} \quad (15)$$

where $M = -f_2/f_1$. Obviously, through changing the beam's phase, the TIM can convert the beam spot diameter from ω' to ω'' with convention relationship $\omega'' = \omega'/M$. From the schematic diagram of the BCRB system presented in Fig. 2. The system consists of a reflector M1, M2, a TIM, and a gain medium. In these elements, the smallest aperture which will produce the beam loss is the gain medium [15]. Therefore, the TIM is set on the side of the gain medium close to the

receiver. According to Section II.C, when ω'' is smaller than the gain section radius a_g , most of the beam can receive by the gain with low beam loss.

In summary, when the beam is reflected back from the receiver, the divergent and enlarged beam caused by long-distance transmission will be compressed by the TIM before it enters the gain medium. As a result, the transmission loss of the system is restrained, which will enhance the transmission distance of the system.

C. Energy Output and Data Receiving

After the processes of energy-absorbing and stimulated radiation, the resonant beam generates and cyclically oscillate in end-to-end. In the receiver, part of the beam will emission from the reflector M2 as a function of the external beam. Based on the cyclic beam power principle [22] and RB system structure presented in Section II, the external beam power can be defined as:

$$P_{\text{beam}} = \eta_s (P_{\text{in}} - P_{\text{th}}), \quad (16)$$

where η_s is the slope efficiency, P_{in} is the input power, and P_{th} is the threshold power (only $P_{\text{in}} > P_{\text{th}}$ the beam can be output). Their specific expression are:

$$\begin{cases} \eta_s = \frac{2\eta_c(1 - R_2)}{(\delta_c - \ln R_2)(1 + R_2)} \\ P_{\text{th}} = AI_s \frac{1 - R_2}{1 + R_2} \end{cases}, \quad (17)$$

where η_c expresses the compounded energy conversion efficiency making by pump efficiency, gain absorption efficiency, and photon efficiency; R_2 is the reflectivity of reflector M2; A is the beam spot area; I_s is the saturation intensity; δ_c is the compounded transmission loss consisting of air absorption loss, and beam loss on the aperture. Since the space loss coming from the air absorption factor is small, the transmission loss can be defined as [15]:

$$\delta_c(d) = N e^{-2\pi \frac{a^2}{\lambda L_3}}, \quad (18)$$

where e is the natural constant; N is the scale factor of beam loss; λ is the wavelength of the resonant beam; a_a expresses the aperture radius. Note that due to the function of TIM, the beam is compressed before it enters the gain medium, the transmission loss produced on the gain medium be greatly reduced or negligible to a certain extent. When the end-to-end distance is out of range, the loss may be created by the TIM because it also has a geometric boundary. However, compared with the gain medium, the geometric boundary of the TIM is adjustable and large.

In the proposed scheme, to achieve information and energy transfer simultaneously, the external beam output from M2 is divided by a beam splitter. One stream is used for energy harvesting, while the other is used for data receiving.

1) *Energy harvesting*: External beam propagates to the PV cell through the optical waveguide and will be converted to electrical power by photoelectric conversion. The process can be defined as [14]:

$$\begin{cases} P_p = \mu P_{\text{beam}}, \\ P_{\text{out}} = a_1 P_p + b_1, \end{cases} \quad (19)$$

where a_1 and b_1 are the structure compound parameters of the PV cell involving the cells' number, background temperature, absorption efficiency, etc., and μ is the beam split ratio. Furthermore, taking the (16), (17) into (19), we can obtain the end-to-end charging conversion efficiency as:

$$\eta_{E_{out}} = a_1 \mu \left(\frac{2\eta_c(1-R_2)}{(\delta_c - \ln R_2)(1+R_2)} - \frac{C}{P_{in}} \right) + b_1, \quad (20)$$

where $C = \eta_s P_{th}$ is the intercept power introduced for simplified analysis.

2) *Data Receiving*: Avalanche photodiode (APD) [27], [28] is applied in the proposed for receiving the optical signal carried by the external beam, which can be expressed as:

$$\begin{cases} P_d = (1-\mu)P_{beam} \\ P_{data} = \gamma P_d \end{cases}, \quad (21)$$

where γ is the parameter of the optical-to-electrical conversion responsivity of APD. Further, the spectral efficiency of the BCRB system can be described as [29]:

$$\tilde{C} = \frac{1}{2} \log_2 \left(1 + \frac{P_{data}^2}{2\pi e n_t^2} \right), \quad (22)$$

where e is the natural constant and n_t is the communication noise. In the proposed scheme, we only consider ideal AWGN for simple analysis, since the AWGN is easy to analyze and approximate. The shot noise and thermal noise are involved in the AWGN, which satisfies the following relationship as:

$$n_t^2 = n_{shot}^2 + n_{thermal}^2, \quad (23)$$

where the $n_{thermal}$ and n_{shot} are expressed thermal noise and shot noise. Among them, the shot noise can be expressed as [30]:

$$n_{shot}^2 = 2q(P_{data} + I_{bg})B_x, \quad (24)$$

where q is the electron charge, B_x is the bandwidth, I_{bg} is the background current. Then, the thermal noise can be defined as [30]:

$$n_{thermal}^2 = \frac{4KT B_x}{R_L}, \quad (25)$$

where K is the Boltzmann constant, T is the background temperature, and R_L is the load resistor.

IV. NUMERICAL ANALYSIS

In the section above, a distance enhanced BCRB scheme based on the TIM is proposed, and the analytical model is developed. In this section, to evaluate the ability of the BCRB system, we will compare the transmission performance between the original and BCRB systems at first. Then, we will analyze the impact of structure parameters on the transmission distance, beam-compression capabilities, output power and data receiving, giving the achievable performance of the BCRB system.

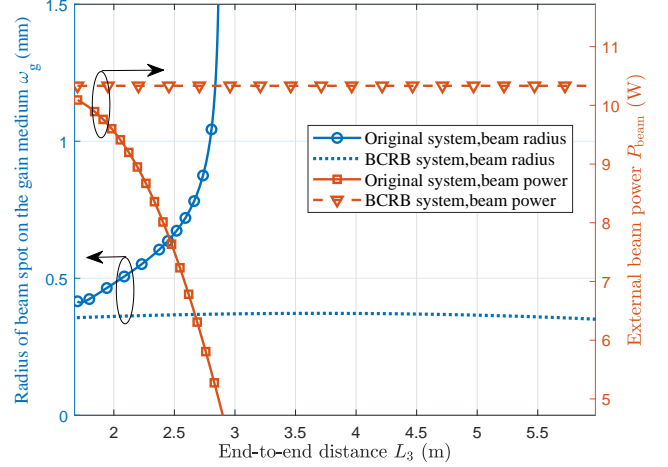


Fig. 8. Beam spot radius on gain medium and external beam power versus end-to-end distance

A. Performance Comparison

According to Section III.B, we can use the beam spot radius to analyze the beam's changing. Moreover, the external beam represents the light ray output from the M2 which will then enter the beam splitter for charging and communication. We can use it to analyze the end-to-end energy transmission. Besides, to directly compare the performance from the original RB scheme, we get the constant parameters from [15], such as the cavity parameters of the original scheme.

1) *Beam spot radius*: We set the M1 and D_0 are adjacent, considering the integration of elements in the transmitter. The curvature radius of M2 takes $\rho_2 = 10$ m. The focal length of D_1 takes $f_1 = -10$ mm. The TIM's parameter takes $M = 3.5$, and the distance between TIM and the left side of the gain medium is set as 100 mm. According to these parameters and the models presented in Section III, the relationship of the spot radius on the gain medium ω_g and end-to-end distance L_3 is given in Fig. 8. As can be seen, the beam spot radius of the proposed system with the TIM can keep less than 0.4 mm, while the original system's beam spot radius is more than 0.4 mm. Moreover, as the values of L_3 increases, the ω_g of BCRB changes smoothly, while the beam spot radius of the original system will drastically increase to 1.5 mm. The numerical results show that the proposed scheme can efficiently compress the incident beam and sustain the compression condition in a variety of ranges.

2) *Transmission distance*: We take the effective reflectivity $R_2 = 0.2618$, the intercept power $C = -51.83$ W, the input power $P_{in} = 210$ W, and the compounded energy conversion efficiency $\eta_c = 0.3384$ [15]; and we set the geometric aperture radius of the TIM as 10 mm. Then, the relationship between the external beam power P_{beam} and the transmission distance L_3 of the system can be depicted. In Fig. 8, the external beam power of the BCRB system with TIM can remain at 10.3 W with the increase of the distance from 1.5 to 6 m, which proves the diffraction loss is effectively reduced through the beam compression. In contrast, P_{beam} of the original decreases

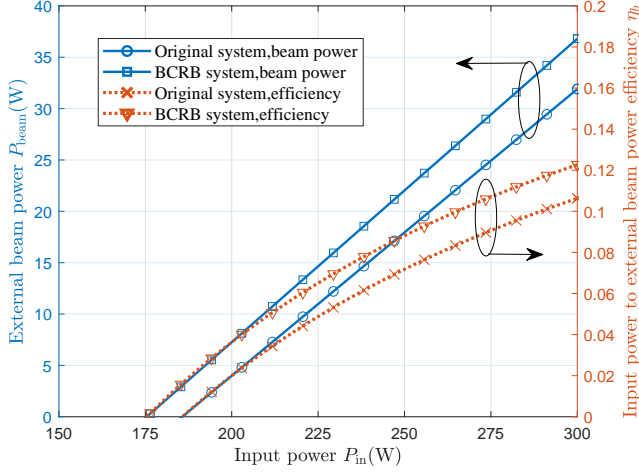


Fig. 9. External beam power and beam conversion efficiency versus input power

nearly 50% to 5 W at $L_3 = 3$ m which presents a high power attenuation. Obviously, the BCRB scheme outperforms the original in energy and beam transmission.

3) *External beam power*: Further, we take $L_3 = 2.6$ m as a reference point [15]. The relationship of external beam power, energy conversion efficiency, and input power can be presented in Fig. 9. As is shown in straight lines, the beam power of both systems linearly increases with the P_{in} charging from 150 W to 300 W. However, the two systems have differences in threshold power and slope efficiency, where BCRB has lower threshold power and higher slope efficiency, presenting a better beam power performance. Moreover, the energy conversion efficiency of systems presents a non-linear trend with the P_{in} increasing. As the value of P_{in} increases, η_b tends to flatten out. In numerical, when P_{in} is 300 W, the conversion efficiency of the BCRB system can be 0.12 while the original system is 0.1. The reduction of transmission loss is beneficial to the improvement of conversion efficiency.

In summary, compared with the original system, the BCRB system can achieve effective and steady beam-compression, which makes the system can transmit beam with energy and signal over a longer distance. Overall, BCRB shows an enhanced transmission performance.

B. Achievable Performance of BCRB System

In this part, through analyzing the stable condition, the beam spot radius, the output power, and the spectral efficiency, we will further evaluate the achievable performance of the BCRB system. The obtained relationship between system performance and parameters has guiding value for system design and optimization.

1) *Stable transmission distance*: Stable condition is the prerequisite for system operation, which ensures the beam oscillation between the receiver and the transmitter. We can get the maximum stable transmission distance through the inequality of stable conditions presented in Section III. Besides, considering some parameters are constant and have no direct

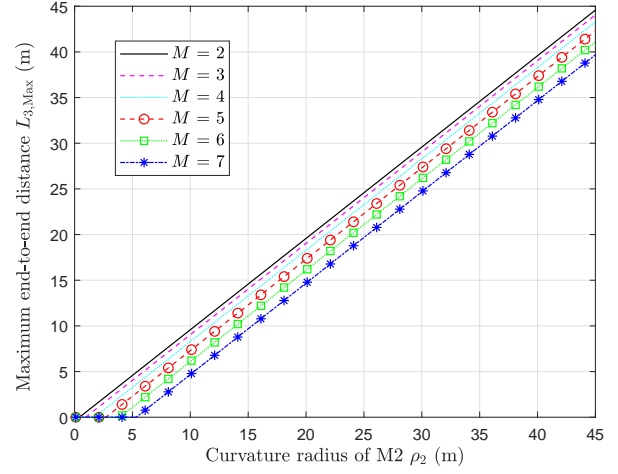


Fig. 10. Maximum end-to-end distance versus curvature radius of M2

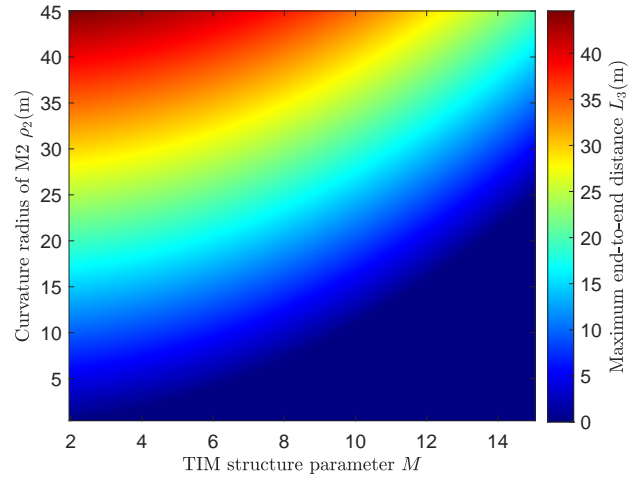


Fig. 11. Maximum end-to-end distance intensity distribution on different ρ_2 and L_3

impact on the stable condition, we mainly evaluate the impact of M and ρ_2 on the BCRB system.

Based on the parameters' value set in the above section, the relationship between curvature radius ρ_2 , TIM's structure parameter M , and the maximum transmission distance $L_{3,Max}$ of the system is shown in Fig. 10. Firstly, values of $L_{3,Max}$ present linearly increasing as ρ_2 increases. Moreover, when the value of parameter ρ_2 is fixed, $L_{3,Max}$ decreases with the increase of M . The curves move downward as M increases, generally. From the analysis model in Section III, the parameter $M = -f_2/f_1$, and f_1, f_2 are characteristic parameters of TIM which determine the optical capability of the lenses. Thus, the change of M will impact the system. Besides, according to the principles of optics [26], the beam will diverge along with the transfer and its curvature of the wavefront will be increased. Thus, the reflective surface of reflector M2 is supposed to have a large curvature to support effective beam reflecting.

To further analyze the impact of M and ρ_2 on the system,

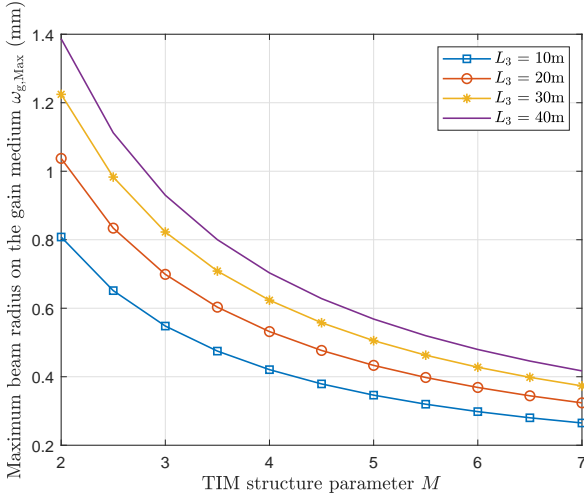


Fig. 12. Maximum beam spot radius on the gain medium versus TIM structure parameter at different distance

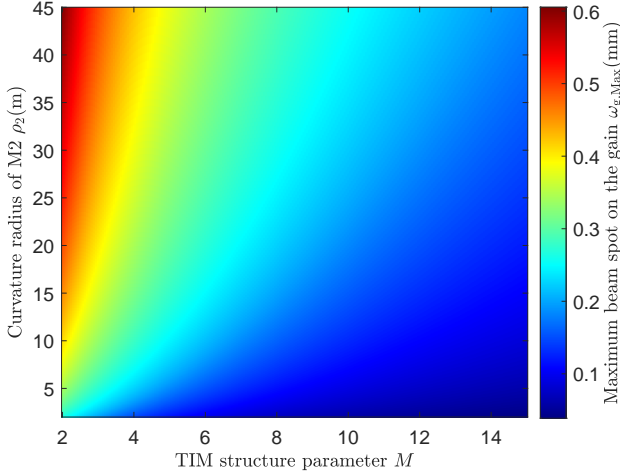


Fig. 13. Maximum beam spot radius on the gain medium intensity distribution on different M and ρ_2

We expanded the range of parameter values (M & ρ_2), and comprehensively considered the influence of the two parameters on $L_{3,Max}$, and obtained the intensity distribution diagram of $L_{3,Max}$ as shown in Fig. 11. Obviously, both the M and ρ_2 impact the $L_{3,Max}$. In numerical, a high value of ρ_2 is beneficial to $L_{3,Max}$. Thus, when the value of M is fixed, to keep $L_{3,Max}$ taking a large value and ensure the stable condition, ρ_2 needs to match a large value.

2) *Beam spot radius*: The compression limit and influencing factors need further analyze. Considering the beam spot radius will be different at different distances, we use the maximum value of the spot radius $\omega_{g,Max}$ on the gain medium to analyze. Furthermore, we set $L_3 = 10, 20, 30, 40$ m as evaluation point. Based on (6), (13), Table I, and the parameters determined above, the relationship curves between $\omega_{g,Max}$ and M can be obtained.

In Fig. 12, the curves present a sharp downtrend at first, and then the decline becomes smooth gradually. When L_3 takes

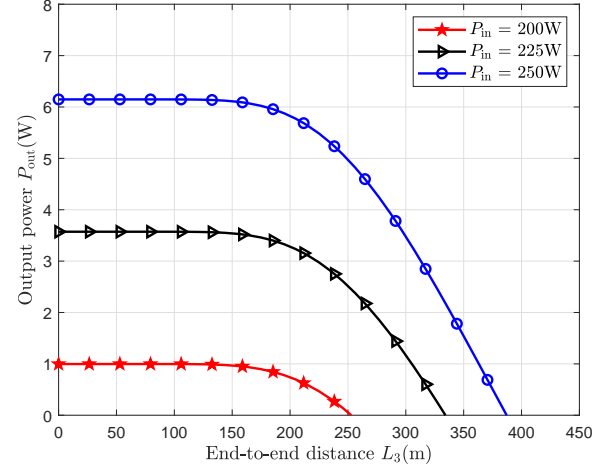


Fig. 14. Output power versus end-to-end distance at different input power

a constant value, the maximum beam spot radius $\omega_{g,Max}$ will decrease with the increase of M , and if M is fixed, $\omega_{g,Max}$ will increase with the L_3 gaining. Overall, M affects the compression capability, a large value of M leads to greater beam compression. However, the incident beam can not achieve unlimited compression through increasing M . According to Section III, factors such as reflector curvature may also affect the beam compression. To assess the level of their influences, the intensity variation of $\omega_{g,Max}$ on M and ρ_2 is presented in Fig. 13. Both the M and ρ_2 have an effect on the $\omega_{g,Max}$. In numerical terms, a high value of M is advantageous to $\omega_{g,Max}$ being small. As a result, while the value of ρ_2 is fixed, M must match a large value in order to keep $\omega_{g,Max}$ obtaining a small value for effective beam compression.

Generally, we can strengthen the compression capability by adjusting the parameter M in a reasonable range.

3) *Power output*: Through the function of the beam splitter, one part of the external beam will be delivered into the PV cells for power output, the rest will be detected by APD for data receiving. To evaluate the performance of the power output, we set the $\mu = 1$ which means all the external beam energy deliver to PV at this time. Then, we take the parameters of the PV cell $a_1 = 0.3487$, and $b_1 = -1.535$ from [15], and set the different boundary parameters P_{in} . The relationship between the output power P_{out} and transmission distance L_3 can be obtained. As shown in Fig. 14, with the increase of end-to-end distance, the values of P_{out} in the BCRB scheme can maintain a certain value in a long-range. Then, after passing through the critical point, the curve of P_{out} presents a downtrend and will reduce to 0 W. Moreover, when P_{in} takes a small value, the entire curves of P_{out} will move down, and the range of the transmission distance constricts slightly. Numerically, P_{out} can be 6 W when the value of P_{in} takes 250 W, and the stable power output range can nearly reach to 200 m.

4) *Data receiving*: The proposed system can effectively enhance the transmission performance, which will also benefit the data transfer. We take optical-to-electrical conversion

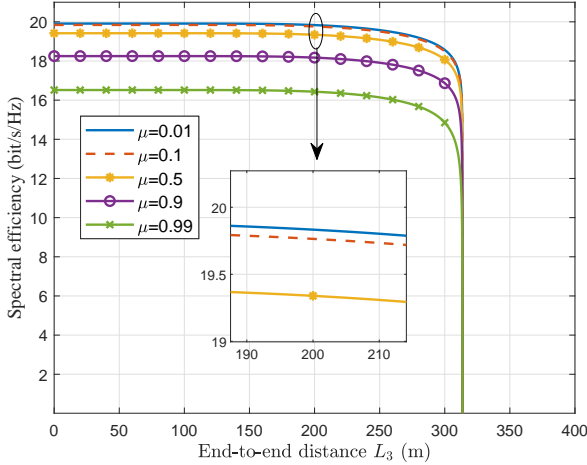


Fig. 15. Spectral efficiency versus end-to-end distance with different split ratio

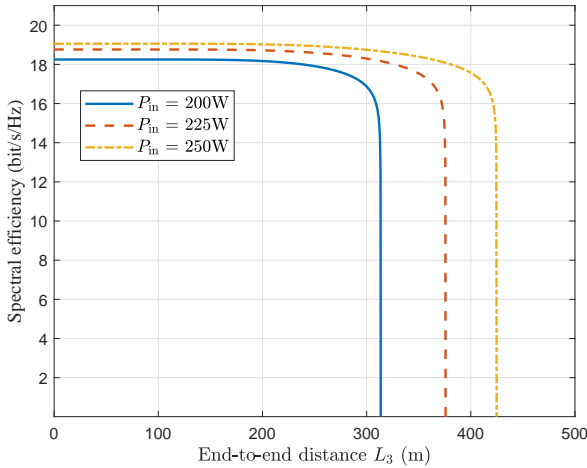


Fig. 16. Spectral efficiency versus end-to-end distance with different input power

responsivity of APD $\gamma = 0.6$ A/W [31], the bandwidth of the noise $B_x = 811.7$ MHz [32], the electron charge $q = 1.6 \times 10^{-6}$ C, the background current $I_{bg} = 5100 \mu\text{A}$ [33], the Boltzmann constant $K = 1.38 \times 10^{-23}$ J/K, the background temperature $T = 300$ K, and load resistor $R_L = 10$ K Ω [30]. Besides, we set the input power $P_{in} = 200$ W, and take split ratio $\mu = 0.01, 0.1, 0.5, 0.9$ and 0.99 . Based on (21)-(24), the relationship between the spectral efficiency \tilde{C} and transmission distance L_3 with different split ratio μ can be described in Fig. 15. As is shown, when the μ is fixed, the curves present a trend of smooth changes firstly and then decreases sharply. Overall, the spectral efficiency can maintain a certain value in a large range of distance, which proves the system's stability. What's more, when the value of μ decreases, the spectral efficiency increases, and curves move up. When the $P_{in} = 200$ W, the spectral efficiency changes from 18-20 bit/s/Hz with different value of μ .

To further explore the impact of input power on spectral

efficiency, we set the split $\mu = 0.9$ as a reference point, and take input power $P_{in} = 200, 225$ and 250 W. After the parameters substitution and formula calculation, the relationship between the spectral efficiency \tilde{C} and transmission distance L_3 with different input power P_{in} is obtained in Fig. 16. As is presented, with the increase of the P_{in} , the BCRB system can achieve a large value of spectral efficiency \tilde{C} accompany by a longer range of the transmission distance. It proves that high input power benefits the improvement of the transmission range and the spectral efficiency.

In summary, calculation results above show that the proposed BCRB system has the capability to supply stable high power output and data receiving over long distances.

V. CONCLUSIONS

To enhance the transmission performance of the resonant beam SWIPT systems, a beam-compress resonant beam (BCRB) scheme is proposed in this paper. Based on the telescope internal modulator (TIM), the divergence of the resonant beam is compressed, and the transmission loss is restrained, which realizes the long-range transfer for the optical wireless information and power. An analytical model of the BCRB system has been developed to evaluate system stability, transmission distance, beam spot, output power, and spectral efficiency and optimize the structure parameters. Numerical results illustrate that the proposed BCRB system can transfer 6 W power and enable 18 bit/s/Hz spectral efficiencies over 200 m, which significantly outperforms the existing RB systems.

REFERENCES

- [1] R. Zhang and C. K. Ho, "MIMO broadcasting for simultaneous wireless information and power transfer," *IEEE Transactions on Wireless Communications*, vol. 12, no. 5, pp. 1989–2001, Mar. 2013.
- [2] K. Georgiou, S. Xavier-de Souza, and K. Eder, "The IoT energy challenge: A software perspective," *IEEE Embedded Systems Letters*, vol. 10, no. 3, pp. 53–56, Jun. 2017.
- [3] K. David and H. Berndt, "6G Vision and Requirements: Is There Any Need for Beyond 5G?" *IEEE Vehicular Technology Magazine*, vol. 13, no. 3, pp. 72–80, July. 2018.
- [4] M. S. Bahbahani and E. Alsusa, "A cooperative clustering protocol with duty cycling for energy harvesting enabled wireless sensor networks," *IEEE Transactions on Wireless Communications*, vol. 17, no. 1, pp. 101–111, Jan. 2018.
- [5] K. Wang, Y. Wang, Y. Sun, S. Guo, and J. Wu, "Green industrial internet of things architecture: An energy-efficient perspective," *IEEE Communications Magazine*, vol. 54, no. 12, pp. 48–54, Dec. 2016.
- [6] K. Huang and E. Larsson, "Simultaneous information and power transfer for broadband wireless systems," *IEEE Transactions on Signal Processing*, vol. 61, no. 23, pp. 5972–5986, Dec 2013.
- [7] N. Shinohara, *Wireless power transfer via radiowaves*. Wiley Online Library, 2014.
- [8] H. Haken, "Laser theory," in *Light and Matter Ic/Licht und Materie Ic*. Springer, 1970, pp. 1–304.
- [9] Q. Liu, J. Wu, P. Xia, S. Zhao, W. Chen, Y. Yang, and L. Hanzo, "Charging unplugged: Will distributed laser charging for mobile wireless power transfer work?" *IEEE Vehicular Technology Magazine*, vol. 11, no. 4, pp. 36–45, Dec 2016.
- [10] M. Liu, H. Deng, Q. Liu, J. Zhou, M. Xiong, L. Yang, and G. B. Giannakis, "Simultaneous mobile information and power transfer by resonant beam," *IEEE Transactions on Signal Processing*, pp. 1–1, May 2021.
- [11] M. A. Khalighi and M. Uysal, "Survey on free space optical communication: A communication theory perspective," *IEEE communications surveys & tutorials*, vol. 16, no. 4, pp. 2231–2258, 2014.
- [12] W. Chen, S. Zhao, Q. Shi, and R. Zhang, "Resonant beam charging-powered UAV-assisted sensing data collection," *IEEE Transactions on Vehicular Technology*, pp. 1–1, Oct. 2019.

- [13] Q. Zhang, W. Fang, Q. Liu, J. Wu, P. Xia, and L. Yang, "Distributed laser charging: A wireless power transfer approach," *IEEE Internet of Things Journal*, vol. 5, no. 5, pp. 3853–3864, Oct. 2018.
- [14] Q. Zhang, W. Fang, M. Xiong, Q. Liu, J. Wu, and P. Xia, "Adaptive resonant beam charging for intelligent wireless power transfer," *IEEE Internet of Things Journal*, vol. 6, no. 1, pp. 1160–1172, Feb. 2018.
- [15] W. Wang, Q. Zhang, H. Lin, M. Liu, X. Liang, and Q. Liu, "Wireless energy transmission channel modeling in resonant beam charging for IoT devices," *IEEE Internet of Things Journal*, vol. 6, no. 2, pp. 3976–3986, Apr. 2019.
- [16] M. Xiong, Q. Liu, M. Liu, X. Wang, and H. Deng, "Resonant beam communications with photovoltaic receiver for optical data and power transfer," *IEEE Transactions on Communications*, vol. 68, no. 5, pp. 3033–3041, Feb. 2020.
- [17] M. Xiong, M. Liu, Q. Zhang, Q. Liu, J. Wu, and P. Xia, "TDMA in adaptive resonant beam charging for IoT devices," *IEEE Internet of Things Journal*, vol. 6, no. 1, pp. 867–877, Feb. 2019.
- [18] W. Fang, Q. Zhang, Q. Liu, J. Wu, and P. Xia, "Fair scheduling in resonant beam charging for IoT devices," *IEEE Internet of Things Journal*, vol. 6, no. 1, pp. 641–653, Feb. 2019.
- [19] W. Fang, H. Deng, Q. Liu, M. Liu, Q. Jiang, L. Yang, and G. B. Giannakis, "Safety analysis of long-range and high-power wireless power transfer using resonant beam," *IEEE Transactions on Signal Processing*, May. 2021.
- [20] A. Al-Kinani, C.-X. Wang, L. Zhou, and W. Zhang, "Optical wireless communication channel measurements and models," *IEEE Communications Surveys & Tutorials*, vol. 20, no. 3, pp. 1939–1962, May. 2018.
- [21] M. Eichhorn, *Laser physics: from principles to practical work in the lab*. Springer Science & Business Media, 2014.
- [22] W. Koechner, *Solid-state laser engineering*. Springer, 2013, vol. 1.
- [23] R. N. N. Hodgson and I. H. Weber, *Laser Resonators and Beam Propagation*. Springer, 2005, vol. 108.
- [24] H. Kogelnik and T. Li, "Laser beams and resonators," *Appl. Opt.*, vol. 5, no. 10, pp. 1550–1567, Oct. 1966.
- [25] P. Baues, "Huygens' principle in inhomogeneous, isotropic media and a general integral equation applicable to optical resonators," *Opto-electronics*, vol. 1, no. 1, pp. 37–44, Feb. 1969.
- [26] M. Born and E. Wolf, *Principles of optics: electromagnetic theory of propagation, interference and diffraction of light*. Elsevier, 2013.
- [27] M. S. Aziz, S. Ahmad, I. Husnain, A. Hassan, and U. Saleem, "Simulation and experimental investigation of the characteristics of a pv-harvester under different conditions," in *2014 International Conference on Energy Systems and Policies (ICESP)*. IEEE, 2014, pp. 1–8.
- [28] J. C. Campbell, "Recent advances in telecommunications avalanche photodiodes," *Journal of Lightwave Technology*, vol. 25, no. 1, pp. 109–121, Jan. 2007.
- [29] A. Lapidath, S. M. Moser, and M. A. Wigger, "On the capacity of free-space optical intensity channels," *IEEE Transactions on Information Theory*, vol. 55, no. 10, pp. 4449–4461, Oct. 2009.
- [30] F. Xu, M. Khalighi, and S. Bourennane, "Impact of different noise sources on the performance of pin- and apd-based fso receivers," in *Proceedings of the 11th International Conference on Telecommunications*, Jun. 2011, pp. 211–218.
- [31] M. S. Demir, F. Miramirkhani, and M. Uysal, "Handover in vlc networks with coordinated multipoint transmission," in *2017 IEEE International Black Sea Conference on Communications and Networking (BlackSea-Com)*, Jun. 2017, pp. 1–5.
- [32] C. Quintana, Q. Wang, D. Jakonis, X. Piao, G. Erry, D. Platt, Y. Thueux, A. Gomez, G. Faulkner, H. Chun, M. Salter, and D. O'Brien, "High speed electro-absorption modulator for long range retroreflective free space optics," *IEEE Photonics Technology Letters*, vol. 29, no. 9, pp. 707–710, Mar. 2017.
- [33] A. J. Moreira, R. T. Valadas, and A. de Oliveira Duarte, "Optical interference produced by artificial light," *Wireless Networks*, vol. 3, no. 2, pp. 131–140, May. 1997.